Electronic Supplementary Information

Synergistic Effects of Nanodiamond Modified Separators Toward Highly Stable and Safety Lithium Metal Batteries

Ying Zhou[a], Kai Zhao[b], Jiaming Zhang[a], Yu Zhu[b], Yue Ma[a], Hongzhou Zhang[a*], Dawei Song[a], Xixi Shi[a], Lianqi Zhang[a*] and Yi Ding[a]

[a] Tianjin Key Laboratory of Advanced Functional Porous Materials, Institute for New Energy Materials and Low-Carbon Technologies, School of Materials Science and Engineering, Tianjin University of Technology, Tianjin 300384, China.

[b] The Centre of Nanoscale Science and Technology and Key Laboratory of Functional Polymer Materials, Institute of Polymer Chemistry, College of Chemistry, Nankai University, Tianjin, 300071, China.

*Address correspondence to: tianjinzhanglq@163.com

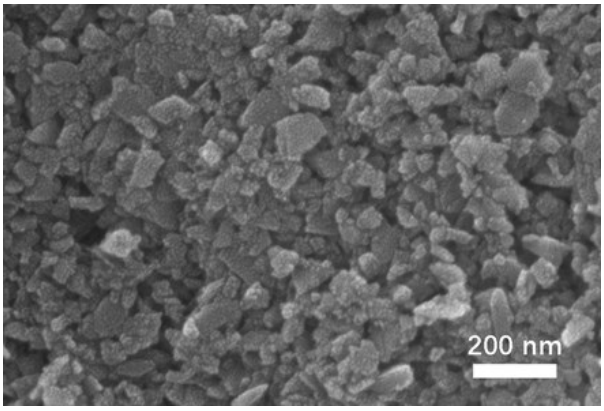

Figure S1. SEM image of the commercial ND.

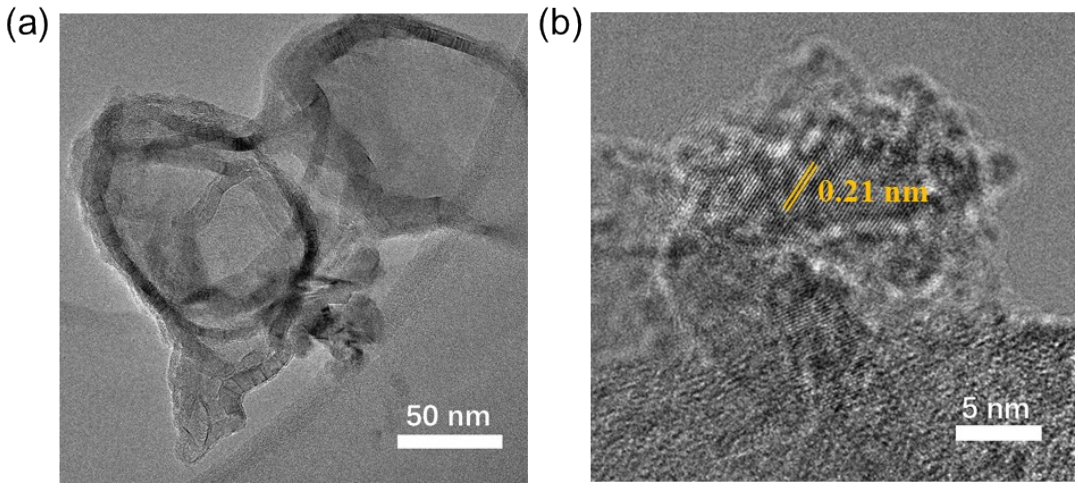

Figure S2. HRTEM images of the commercial ND under different magnification. The interplanar crystal spacing was measured to be 0.21 nm, corresponding to (111) plane of the diamond.[1]

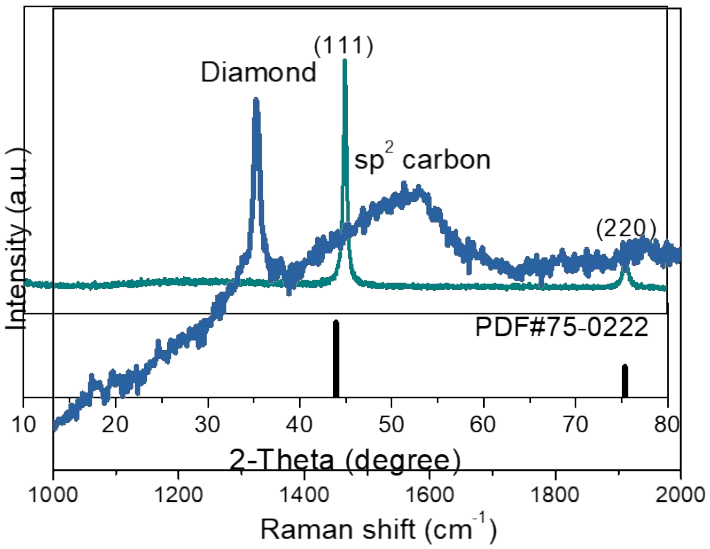

Figure S3. XRD pattern of the ND.

Figure S4. Raman pattern of the ND. The peak at 1322 cm^{-1} shows the characterization peak of the diamond. The broad peak at about 1580 cm^{-1} is the characterization peak of sp^2 carbon, corresponding to the graphite on the ND surface.[2,3]

Figure S5. Optical image of the final ND dispersion with the concentration of 2 mg mL^{-1}.

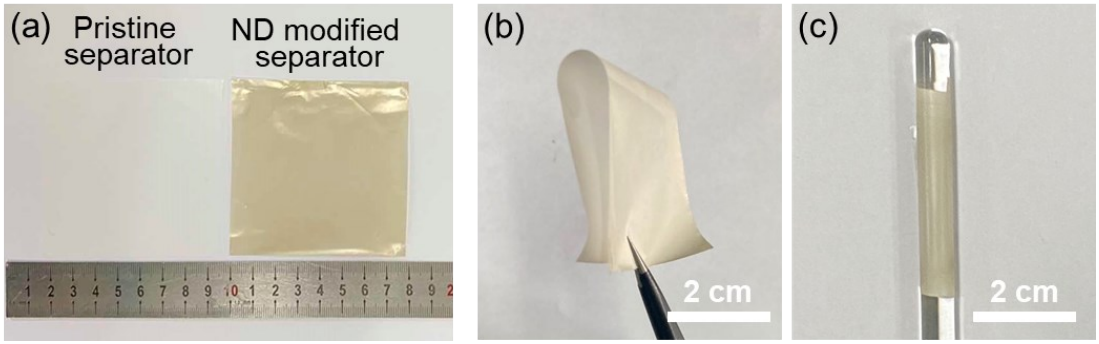

Figure S6. (a) Optical images of the pristine separator (left) and the ND modified separator (right). The optical images showing the (b) bending and (c) coiling modes of the ND modified separator, which prove its good flexibility.

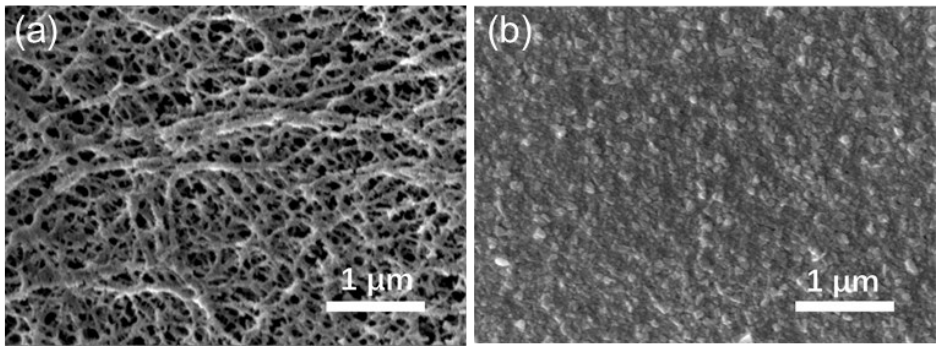

Figure S7. SEM images of the ND modified separator for the side (a) without the ND and (b) with the ND.

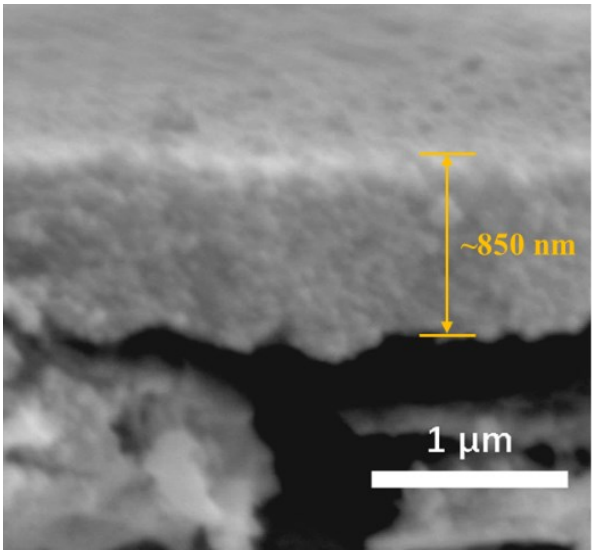

Figure S8. Cross-sectional view SEM image of the ND layer.

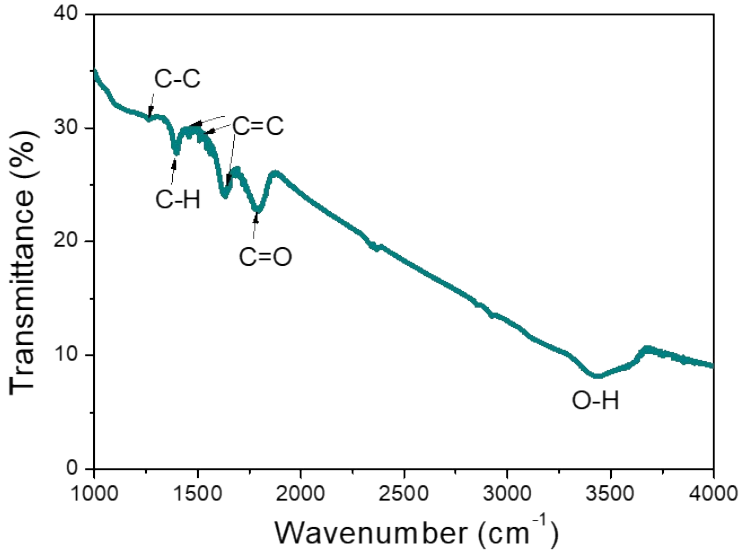

Figure S9. FTIR pattern of the ND. Result shows the existence of C=O and O-H characteristic peaks.[4]

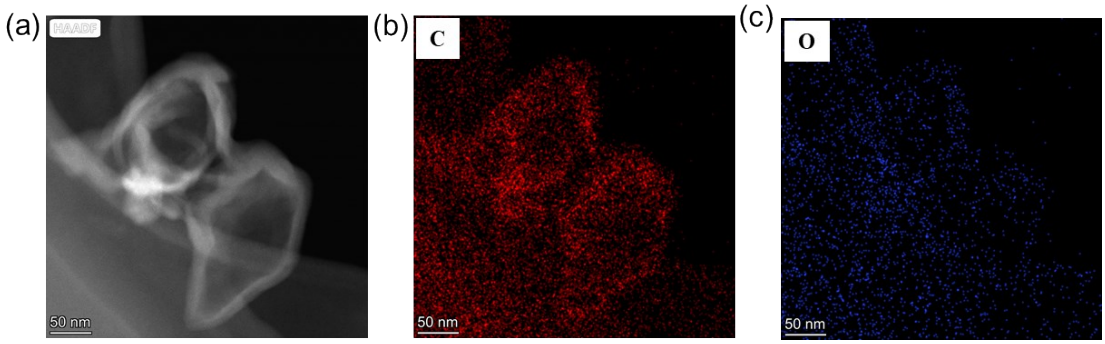

Figure S10. (a) HRTEM image and (b-c) the corresponding EDS results of the ND. The elements C (93.7 at%) and O (6.3 at%) are detected.

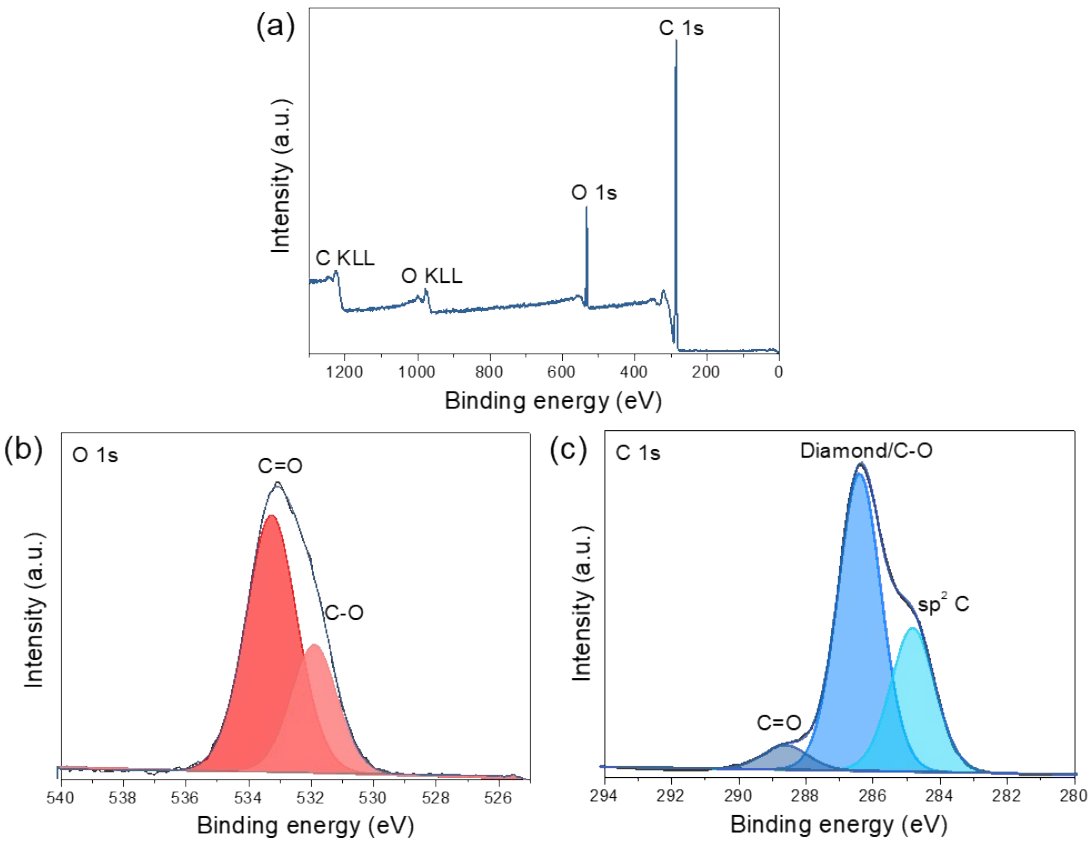

Figure S11. (a) XPS survey spectra of the ND and the corresponding high-resolution (b) O 1s and (c) C 1s spectra. The elements C (89.3 at%) and O (10.7 at%) are detected and the atomic ratio result is close to the EDS result. The O 1s spectrum can be deconvoluted into two peaks at 533.2 eV and 531.8 eV, assigning to the characteristic peak of C=O and C-O.

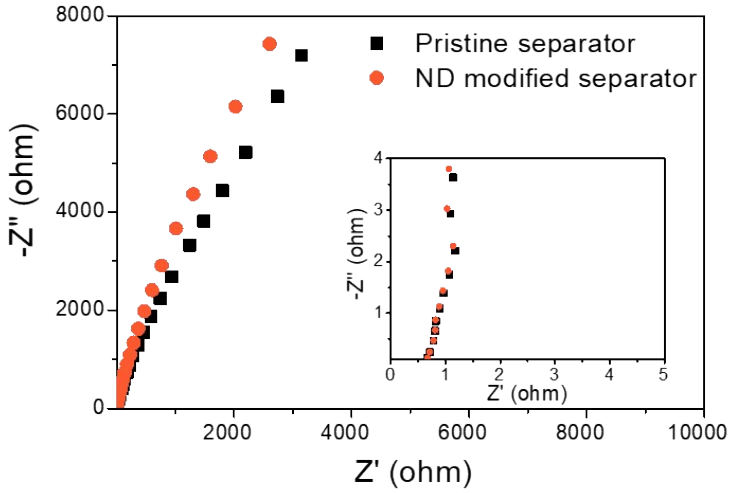

Figure S12. Nyquist plots of stainless steel|separator|stainless steel block cells with the pristine separator (black) and ND modified separator (red). The ionic conductivity of the ND modified separator with the electrolyte is determined to be 1.26 mS cm^{-1}, and the ionic conductivity of the pristine separator is determined to be 1.20 mS cm^{-1}.

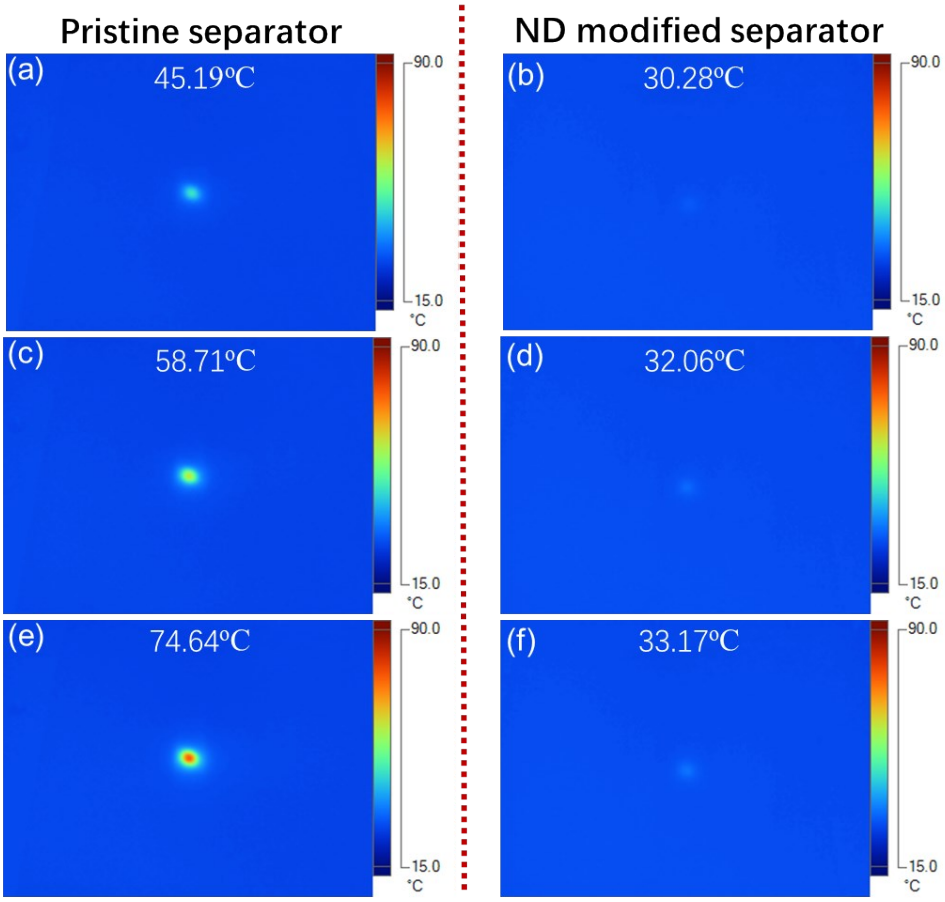

Figure S13. Typical temperature profiles of the (a, c, e) pristine separator and (b, d, f) ND modified separator with the power of (a, b) 50 mW, (c, d) 65 mW and (e, f) 78 mW. The corresponding peak temperature within the heating area is shown in the top site of each image.

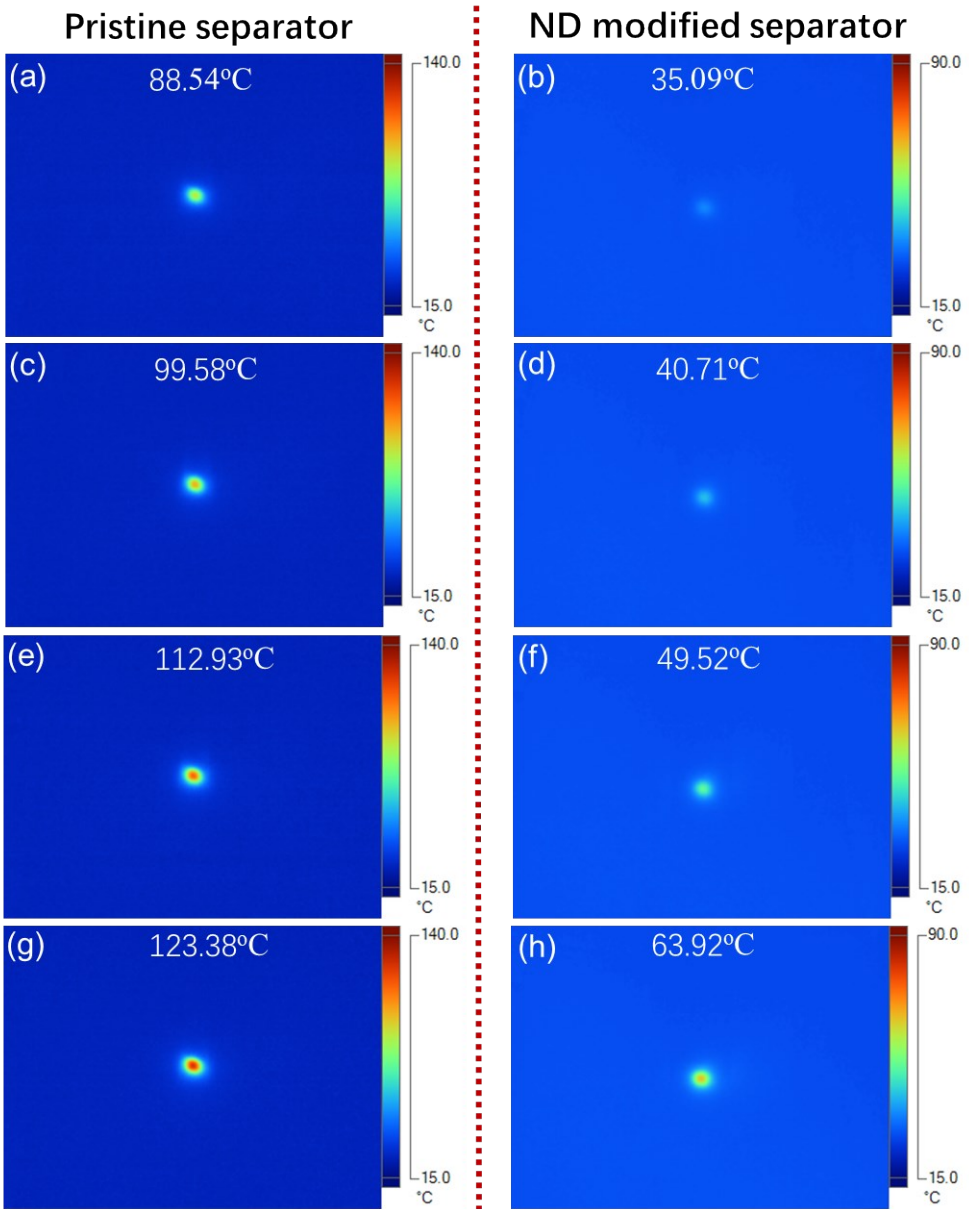

Figure S14. Typical temperature profiles of the (a, c, e, g) pristine separator and (b, d, f, h) ND modified separator with the power of (a, b) 88 mW, (c, d) 104 mW, (e, f) 118 mW and (g, h) 131 mW. The corresponding peak temperature within the heating area is shown in the top site of each image.

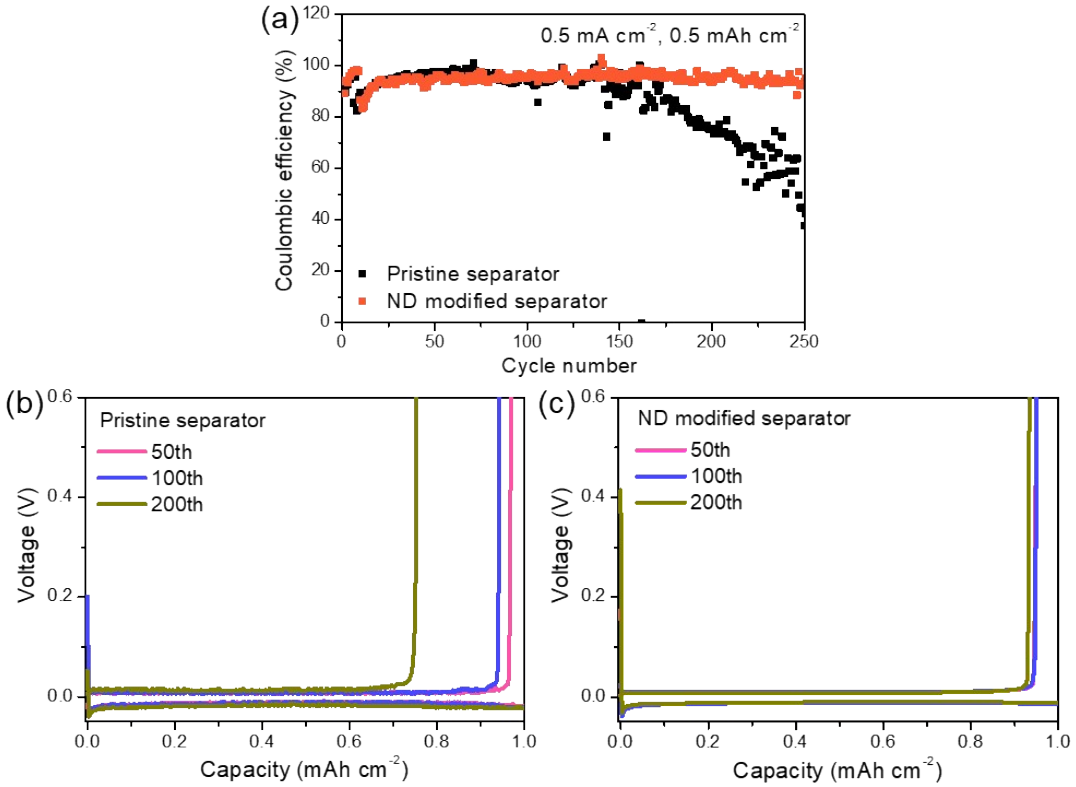

Figure S15. (a) Coulombic efficiency tests in Li|Cu cells assembled with the pristine separator and ND modified separator at 0.5 mA cm^{-2} with an areal capacity of 0.5 mAh cm^{-2}. Voltage profiles of Li plating/stripping processes in Li|Cu cells assembled with the (b) pristine separator and (c) ND modified separator with an areal capacity of 0.5 mAh cm^{-2} at 0.5 mA cm^{-2}.

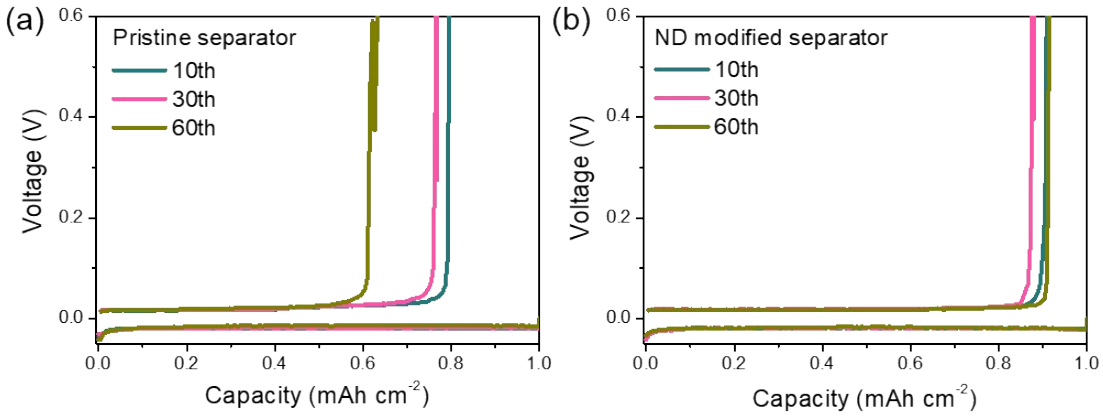

Figure S16. Voltage profiles of Li plating/stripping processes in Li|Cu cells assembled with the (a) pristine separator and (b) ND modified separator with an areal capacity of 1 mAh cm^{-2} at 2 mA cm^{-2}.

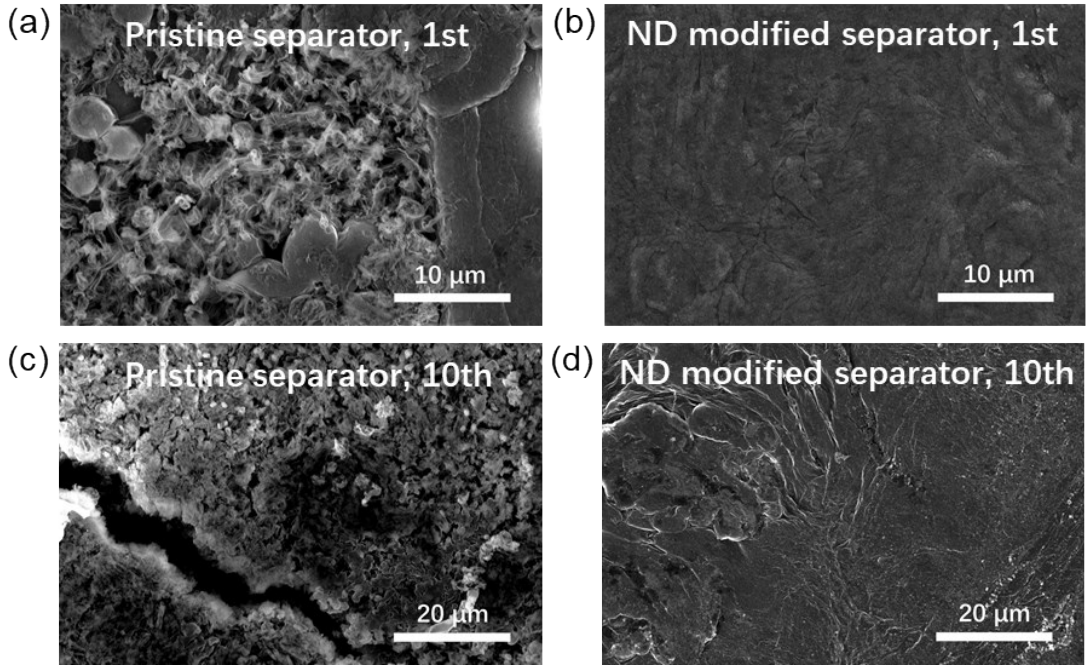

Figure S17. Magnified SEM images of Li metal anodes in symmetric cells assembled with the (a, c) pristine separator and (b, d) ND modified separator after (a, b) 1 cycle and (c, d) 10 cycles.

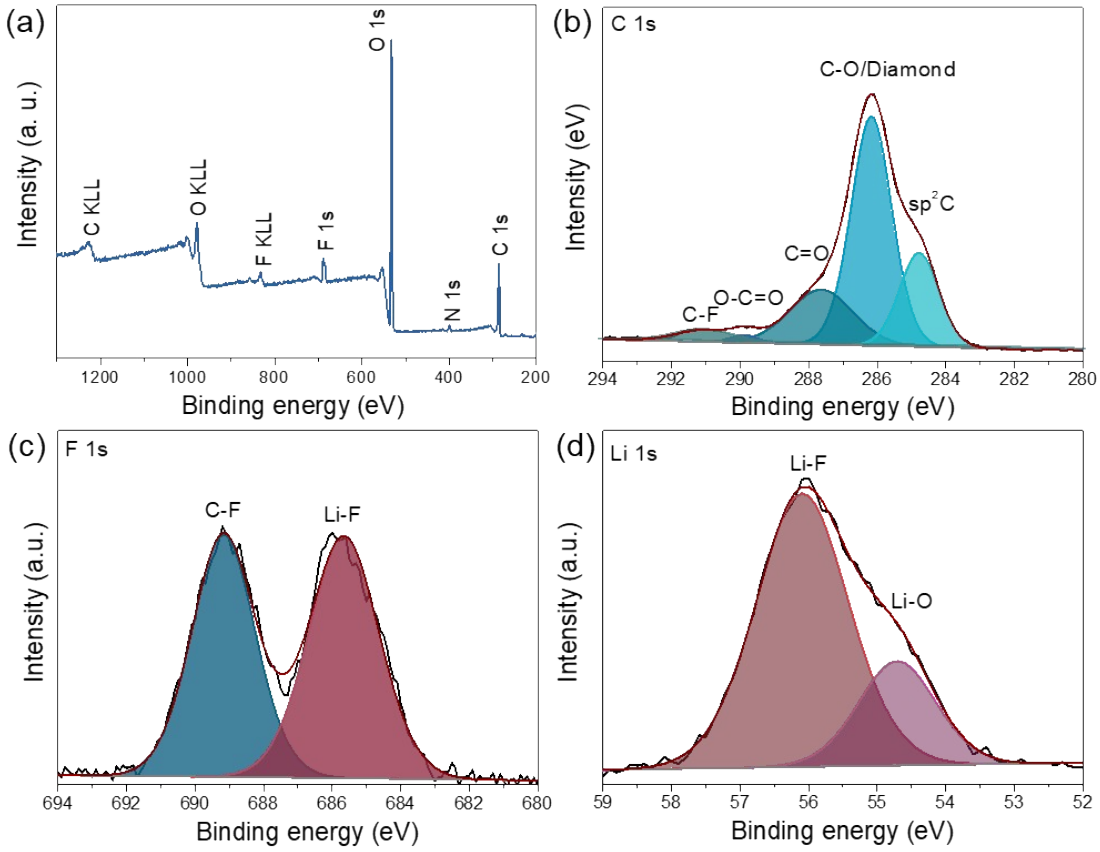

Figure S18. (a) XPS survey spectrum, (b) C 1s, (c) F 1s and (d) Li 1s spectra and their fitting curves of the SEI layer of Li metal anode in symmetric cell assembled with the ND modified separator after cycling for 10 cycles. The peak at 286.2 eV of the C 1s spectrum exhibits the existence of both C-O and sp^3 carbon, proving that a small amount of ND particles will drop from the separator and deposit on the Li surface, and this may also benefit for the uniform Li deposition.[1,5]

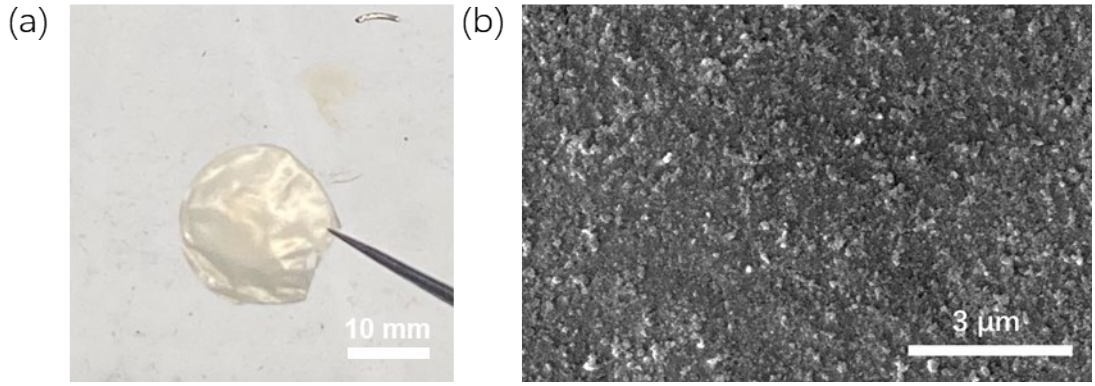

Figure S19. (a) The optic image of the ND modified separator after cycling, the damaged edge was caused by disassembled process of the cell. (b) SEM image for the ND side of the ND modified separator after cycling for 10 cycles in symmetric cell.

References	LFP Mass Loading	Li Anode	Test Condition	Capacity Retention	Electrolyte
Overoxidised polypyrrole separator[6]	2 mg cm^{-2} 10 mg cm^{-2}	Commercial Li foil	0.5 C, 470 cycles 0.5 C, 100 cycles	About 80% according the given profile 89%	1 M $LiPF_6$ in EC/DEC(1:1 wt)
$MnCO_3$@PP separator[7]	3.8 mg cm^{-2}	Commercial Li foil 2 mAh cm^{-2}	0.5 C, 800 cycles 0.5 C, 250 cycles	90.7% 97.4%	1 M $LiPF_6$ in EC/DMC(1:1 vol)
Poly(ether ether ketone) separator[8]	2 mg cm^{-2}	Commercial Li foil	2 C, 580 cycles	65.2%	1 M $LiPF_6$ in EC/DEC/DMC (1:1:1 vol)

HAPs/PVA separator[9]	1-1.2 mg cm^{-2}	Commercial Li foil	0.2 C, 100 cycles	97.3%	1 M $LiPF_6$ in EC/DMC(1:1 vol)
Nanocellulose modified separator[10]	1.5 mg cm^{-2}	Commercial Li foil	0.5 C, 65 cycles	97.5%	1 M $LiPF_6$ in EC/DEC(1:1 wt)
Functionalized nanocarbon coated separator[11]	Not provided	Commercial Li foil	1 mA cm^{-2}, 856 cycles 1 mA cm^{-2}, 819 cycles 1 mA cm^{-2}, 793 cycles	80% 80% 80%	1 M LiTFSI in DOL/DME (1:1) 1.2 M $LiPF_6$ in EC/EMC (3:7) 1 M $LiClO_4$ EC:PC (1:1)
Regenerated eggshell membrane[12]	1.6-1.8 mg cm^{-2}	Commercial Li foil	5 C, 200 cycles	78.4%	1M $LiPF_6$ in EC/DEC (1:1 vol)
This work ND modified separator	**3.2 mg cm^{-2}**	**Commercial Li foil**	**2 C, 1000 cycles** **1400 cycles**	**96.2%** **90%**	**1 M LiTFSI in DOL/DME (1:1 vol) + 1wt% $LiNO_3$**

Table S1. Cycling performance comparison of LFP|Li cells with different separators in representative works.

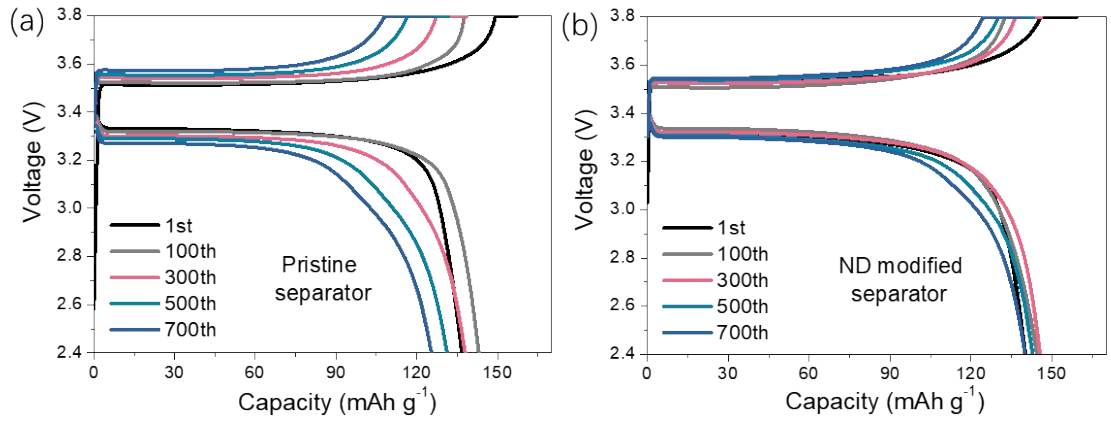

Figure S20. Typical galvanostatic charge-discharge profiles of Li|LFP cells assembled with the (a) pristine separator and (b) the ND modified separator at 2 C after different cycles.

Rate	LFP|Pristine separator|Li (mAh g^{-1})	LFP|ND modified separator|Li (mAh g^{-1})
0.1 C	151.9	163.7
0.2 C	154.8	160.4
0.5 C	153	158.3
1 C	147.7	153.9
2 C	139.7	147.8
5 C	121	134.6
10 C	107.4	117

Table S2. The discharge capacity of LFP|Li cells assembled with the pristine separator and ND modified separator at the 5th cycle of different rate.

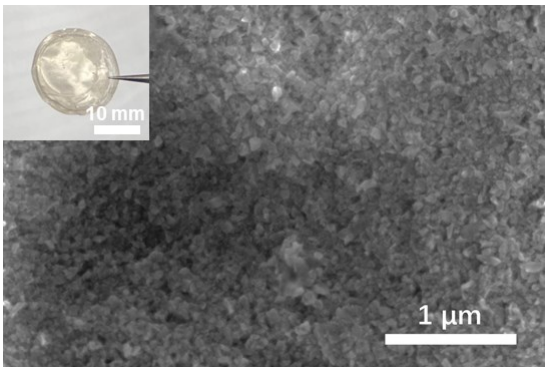

Figure S21. The SEM image for the ND side of the modified separator after cycling for 200 cycles in LFP|Li cell at 2 C. Inset shows the corresponding optic image.

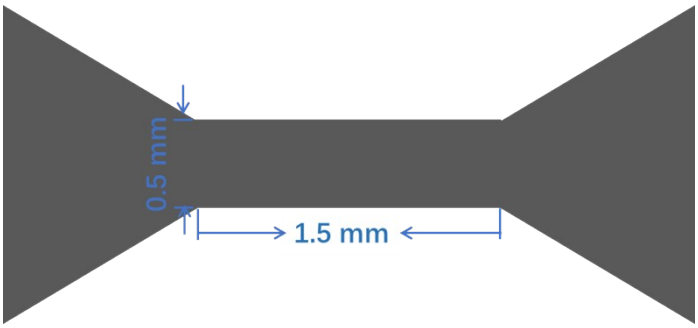

Figure S22. Schematic of the patterned rGO film.

Reference

1. X. Cheng, M. Zhao, C. Chen, A. Pentecost, K. Maleski, T. S. Mathis, X. Zhang, Q. Zhang, J. Jiang and Y. Gogotsi, *Nat. Commun.*, 2017, **8**, 336-336.
2. V. Mochalin, O. Shenderova, D. Ho and Y. Gogotsi, *Nat. Nanotechnol.*, 2012, **7**, 11-23.
3. V. Mochalin, S. Osswald and Y. Gogotsi, *Chem. Mater.*, 2009, **21**, 273-279.
4. S. Osswald, G. Yushin and V. Mochalin, *J. Am. Chem. Soc.*, 2006, **128**, 11635-11642.

5. Z. Shen, W. Zhang, S. Li, S. Mao, X. Wang, F. Chen and Y. Lu, *Nano Lett.*, 2020, **20**, 6606-6613.
6. Z. Wang, R. Pan, C. Xu, C. Ruan, K. Edstr?M, M. Str?Mme and L. Nyholm, *Energy Storage Mater.*, 2018, **13**, 283-292.
7. J. Yan, F. Liu, Z. Hu, J. Gao, W. Zhou, H. Huo, J. Zhou and L. Li, *Nano Lett.*, 2020, **20**, 3798-3807.
8. J. Liu, Y. Mo, S. Wang, S. Ren and Y. Meng, *ACS Appl. Energy Mater.*, 2019, **2**, 3886-3895
9. W. Wang, C. Liao, K. M. Liew, Z. Chen, L. Song, Y. Kan and Y. Hu, J. Mater. Chem. A, 2019, **7**, 6859-6868.
10. R. Pan, X. Xu, R. Sun, Z. Wang, J. Lindh, K. Edström, M. Strømme and L. Nyholm, *Small*, 2018, **14**, 1704371.
11. Y. Liu, Q. Liu, L. Xin, Y. Liu, F. Yang, E. A. Stach and J. Xie, *Nat. Energy*, 2017, **2**, 17083.
12. L. Ma, R. Chen, Y. Hu, W. Zhang, G. Zhu, P. Zhao, T. Chen, C. Wang, W. Yan and Y. Wang, *Energy Storage Mater.*, 2018, 14, 258-266.